

Supplementary material

PPDN, NTCDA anions radical formation in EMIM-DCA, BMIM-BF₄, EMIM-AC ionic liquid solutions under the steady state UV and VIS light illumination: A Combined X-, K-band ESR and DFT Study

A. Konkin^{a*}, U. Ritter^a, A. A. Konkin^{a,b}, A. Knauer^a, V. Krinichnyi^c, V. Klochkov^b, M. Gafurov^b, A. Aganov^b, F. Wendler^d, P. Scharff^a

a) Institute of Micro- and Nanotechnologies MacroNano®, Technische Universität Ilmenau, Gustav-Kirchhoff-Str.7, D-98693 Ilmenau, Germany

b) Institute of Physics, Kazan Federal University, Kremlyovskaya Str. 18, Kazan, Russia

c) Department of Kinetics and Catalysis, Institute of Problems of Chemical Physics RAS, Academician Semenov Avenue 1, 142432 Chernogolovka, Russia

d) TITK, Smartpolymer GmbH, Breitscheidstraße 97, 07407 Rudolstadt/ Thuringen, Germany

SM-1. Light-induced reaction in FD:o-DCB/(EMIM-ac) suspension

The preliminary X-band light-induced EPR (LEPR) in suspension of PCDTBT:PCBM-oDCB solution with BMIM⁺-Ac⁻ ionic liquid has been reported in XXVI international EPR seminar in Graz University and Technology in June 2015 and indicated the degradation of acetate anion in the presence of PCBM electron acceptor under Xe-lamp CW illumination. Due to the lack of an appropriate pdf file on the seminar website <https://ieprs.org/meeting/xxvi-international-epr-seminar-2015/>, a copy of the seminar abstracts is available in SM-4.

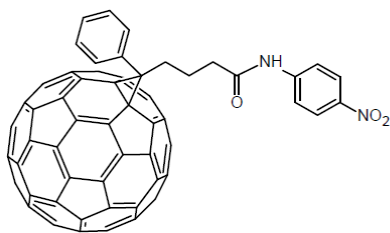
Here, two ionic liquids (EMIM⁺-Ac⁻ and BMIM⁺-SCN⁻, (Fig.S1d,e) were blended with PC₆₀BM-nitroaniline, PC₆₀BM-dispersiongelb and PC₆₀BM (Fig.S1-a,b,c) solution in o-DCB in suspension phase has been studied with the supposition of FD di-anion di-radical formation. The triplet state registration of the fullerene di-anions by means of LEPR has been performed under electrochemical reduction [S1], but has not been observed so far in photo-induced charge separation processes in organic SCs. With regards to oxidation in D/A suspension, fullerenes and their ortho quinodimethane adducts were reduced in photo-excited TiO₂ suspensions and reported in [S2].

SM-1a. Composites utilised in experiments

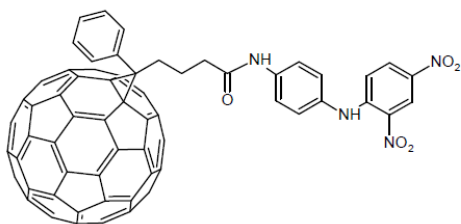
The structures of the new FDs: a) PC₆₀BM-nitroaniline (denominated below as FD₁), b) PC₆₀BM-dispersiongelb (below is FD₂) and c) PC₆₀BM are shown in Fig. S1. The aim to check the new PC₆₀BM derivatives as potential effective electron acceptors is connected with the presence of nitro groups on fullerene side, which increase their electron acceptor strength [S3] and could be considered as possible basic molecules for di-anion formation. For the choice of the polymer, namely, (PCDTBT, Fig. S1f), we only kept in mind that it is an effective electron donor among conjugated polymers [S4], the choice of **IL-2** (Fig.S1e) was based at the result of the sure detection of [•]CH₃ radical generation (see below) under UV light excitation in blend included IL-1 (Fig.S1d). Actually, both ions in IL-1 have -CH₃ fragments, while in IL-2, -CH₃ is only present in the cationic state. The comparison of the light-induced EPR data of both IL-1 and IL-2 in order to examine what ion in ILs is responsible for the [•]CH₃ formation, was in focus at the first step of

the study. Although, IL-1 has no wide applications in comparison with some other ILs, it is however an effective “green” solvent for cellulose in industry [S5,S6,S7] and its photo-stability makes sense, taking into account the probability of photo-electron traps presence in solutions based at IL-1.

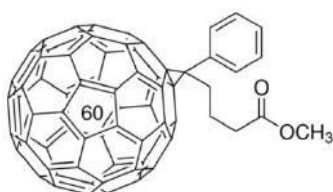
Fullerene derivatives



a) PCBM-nitroaniline (**FD₁**)

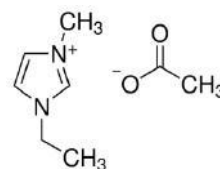


b) PCBM-dispersiongelb (**FD₂**)

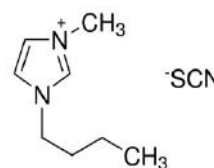


c) PC₆₀BM

Ionic liquids (ILs)

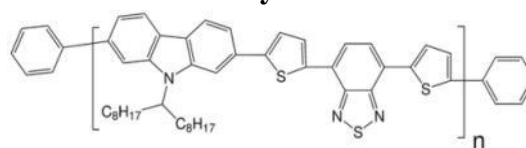


d) 1-Ethyl-3-methylimidazolium acetate (**IL-1**)



e) 1-Butyl-3-methylimidazolium thiocyanate (**IL-2**)

Polymer



f) PCDTBT

Fig. S1

Electron donor and acceptor molecules utilized in D/A blends

With respect to composites, we make a special emphasis on blends feature: FDs and o-DCIB are not soluble in ILs (or possess a very low solubility). Therefore, all experiments were carried out in suspension blends and the results should be assigned to the interface processes i.e. close to the experimental conditions with suspensions of TiO₂ reported in [2]). In order to be sure to perform precise measurements of the compared spectra (resonance field positions), two hyperfine structure (hfs) lines $m=3/2$ and $m=1/2$, of the Cu²⁺(Et₂dtc₂) in benzene solution, denominated in Fig.S2 and Fig.S3 as Cu²⁺L₂ complex, have been used as a reference for the magnetic field position. Their hfc lines are essentially displaced from the studied signal and the Cu²⁺L₂ reference location in the resonator is independent from the position of the studied samples and always recorded at room temperature i.e. outside from Dewar with the samples. And so in all X-band comparative experiments Cu²⁺L₂ hfs lines must be exactly aligned with each other and this coincidence has been corrected before the data handling (light-dark response). In Fig.S2, Fig.S3, and Fig.S4 the following spectra denominations are used: “dark” (recorded without light illumination), “light” (under illumination). All spectra in Fig.S4 are “light-dark” and therefore reference lines of Cu²⁺L₂ are absent. For the light illumination, a CW Xe-lamp (P=150 W) was used.

PCDTBT:PCBM (1:2) solution in o-DCB

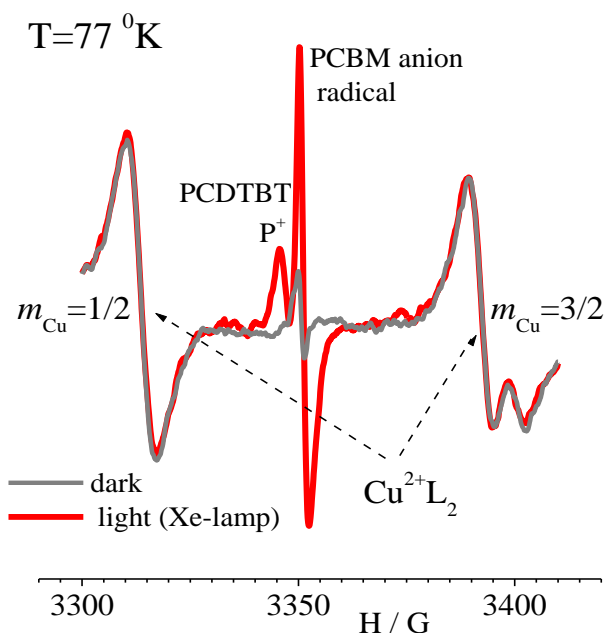


Fig. S2

“dark” and “light” EPR, spectra of PCDTBT:PCBM solution in o-DCB, recorded with two hfc lines of the reference $\text{Cu}^{2+}(\text{Et}_2\text{dtc}_2)$ denominated as Cu^{2+}L_2 .

SM-1b. Results and discussion

LEPR spectrum of PCDTBT:PC₆₀BM (1:1) solution (~1 mmol/L) in o-DCB at 77K is shown in Fig.S3a and demonstrates the typical light-induced response of two overlapped spectra, namely, polymer positive polaron (P^+) and FD anion radical (PCBM in Fig.S3). In frozen suspensions of PCDTBT:PC₆₀BM solution with IL-1 (1:5 volume ratio, v.r.), the line maximum attributed to the P^+ spectrum is displaced at about $\Delta g = 5.4 \cdot 10^{-4}$ (Fig.S3b), which is essential even for X-band EPR. This result is not typical for the P^+ spectra of the polymer in solvents and other additives in frozen solutions and looks unusual. Moreover, the additional spectrum, attributed to $\cdot\text{CH}_3$ was registered as well. The supposition, that both spectral components in the overlapped area P^+ and PCBM $^{\cdot-}$ in Fig.S3b are attributed to R_{FD} anion radicals has been checked in FD/IL blends without polymer under the same experimental conditions and the results are displayed in Fig.S4. The simple comparison of the peak-to-peak distance ΔH in Fig.S3 and in Fig.S4 confirms the supposition of both signal assignments to the FD anion radicals generated in PCBM, FD₁, and FD₂ solutions in o-DCB with IL-1 additive (1/5 v.r.) under CW Xe-lamp illumination. Below, the low field component of the spectra around the centre is assigned to the supposed di-anion di-radical as R_2 , and the high field around the centre of the spectra to the mono anion radical R_1 as shown in Fig.S4. From the spectra in Fig.S4 one can see the evident difference of relative R_1 and R_2 over-distribution in the spectra a), b) and c), that is evident due to the difference of the FDs electron acceptor strengths and is indirectly confirmed by the same tendency of the increasing $\cdot\text{CH}_3$ radical intensity. As it was mentioned above both ions in IL-1 have the methyl fragments, which could be responsible for the $\cdot\text{CH}_3$ radical generation under the UV irradiation. However, the simple substitution of the anionic OCOCH_3 in IL-1 to SCN^- in IL-2 did not indicate a $\cdot\text{CH}_3$ generation under the same light illumination, therefore one can assign the $\cdot\text{CH}_3$ formation to the acetate anion in IL-1. The steps of the photoreaction in FD:IL-1 blend are resulting in the formation of $\cdot\text{OCOCH}_3$ radicals, caused by photo-electron transfer as very short-living intermediates, which could be possibly happen before the $\cdot\text{CH}_3$ radical formation takes place. An attribution of the weak spectra components R_X and R_{X1} , is problematic taking in mind, that the complete spectrum that is related to these weak spectral components is unknown.

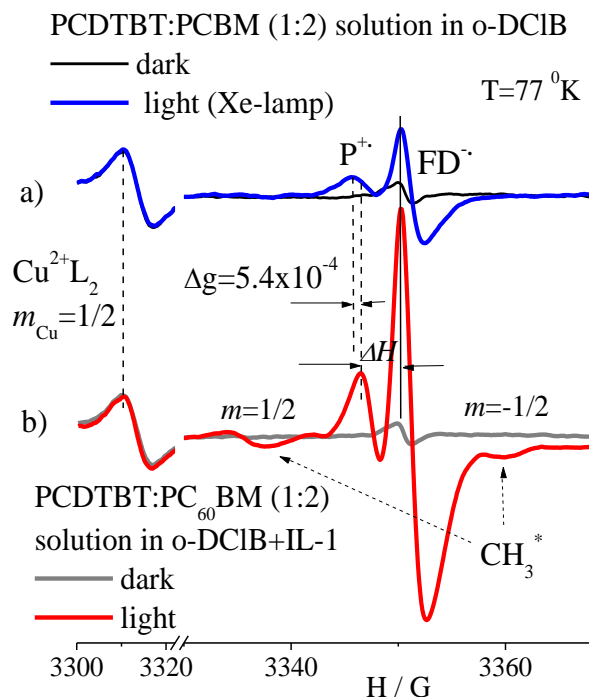


Fig.S3

“dark” and “light” EPR spectra of: a) PCDTBT:PCBM solution in o-DCB, b) PCDTBT:PCBM solution in o-DCB/ IL-1 (1/5).

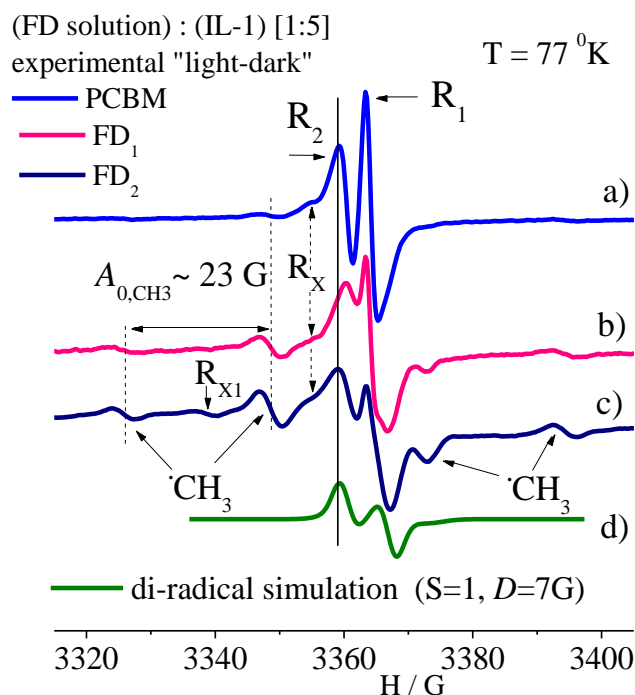


Fig.S4

“light-dark” EPR spectra of FD:o-DCB/IL-1 solution-suspension (v.r. 1/5) of FD: a) PCBM, b) FD1, c) FD2, c) di-radical simulation ($S=1$).

The supposition of ethyl $\text{CH}_3\text{-CH}_2^\bullet$ radical formation by means of the $\bullet\text{CH}_3 + \text{CH}_3 \rightarrow \text{CH}_3\text{-CH}_3$ synthesis [S8a] after the long-lived steady state UV photolysis is not confirmed by the $\text{CH}_3\text{-CH}_2^\bullet$ spectral simulation using H_α and H_β hfc parameters, which are respectively ~ 20 G and ~ 26 G [S8b]. Therefore, the attribution of the weak R_X and R_{X1} spectral components is unknown. By the way, both registered $\bullet\text{CH}_3$ and FD^\bullet are surely stabilised at 77K even after the illumination was switched off.

SM-2 PPDN

SM-2a. PPDN:EMIM-Ac

While the concentration of PPDN^\bullet in EMIM-Ac was around 0.6 mmol/L i.e. near 4 times less than in EMIM-DCA, the formation of PPDN^\bullet in solution under the Xe lamp illumination is reliably registered by EPR and the spectrum recorded at 30°C is introduced in Fig.S5a. The spectrum processing gives $\beta_1 = 0.18$ G and $\delta_1 = 0.47$ G, that are close to the above mentioned values in BMIM-BF₄ i.e. ~ 0.22 G and ~ 0.6 G respectively (see Fig.4b in the main text). This correlation is expected due to the close values of their viscosities, i.e. 103 mPas (BMIM-BF₄) and 93 mPas (EMIM-Ac) corresponding to a temperature of $T=25^\circ\text{C}$. The experimental PPDN^\bullet spectrum in EMIM-Ac solution is described well only by the sum of two spectra (the details are considered below in SI-2b). Unfortunately, the high instability of the EMIM-Ac+EA system arises due to the formation of other photo-induced radical products with increasing temperature (Fig.S5b), namely a degradation of the initial system components that is caused by irreversible reactions and thus, it limits the application of EMIM-Ac in the analyses of diffusion processes. Spectrum in Fig.S5b described equally well by two overlapping isotropic spectra with a difference of the g-factors and linewidths as well as one centrum that can be described by the Dyson line form, that in principle

could be possibly assumed for the long polymer chain or solid domain formation in a highly viscous medium. Therefore, the above mentioned is an obstacle for the understanding the origin of the paramagnetic centrum by EPR only.

SM-2b. PPDN π - π stacking dimer

The experimental PPDN \cdot spectra recorded at temperatures below room temperature, are processed by the superposition of two spectra $X \cdot F_{(M)} + (1-X) \cdot F_{(D)}$, where $F_{(M)}$ is attributed to the PPDN \cdot mono-radical EPR spectrum, $F_{(D)}$ is assigned to the spectrum of relatively short-living π - π stacking dimer (PPDN $\cdot \leftrightarrow$ PPDN \cdot) and X is the monomer relative part. The hfc tensors of the mono and dimer magnetic nucleus differ approximately by a factor 2: $A_{0(D)} \approx 0.5 \cdot A_{0(M)}$. The above could be assigned to the electron hopping between the anion radical and the neutral PPDN with a structure close to a π -stacked dimer and the over-distribution of the electron spin density in the dimer is confirmed by ENDOR in analog systems including a π - π stacking structure [S9].

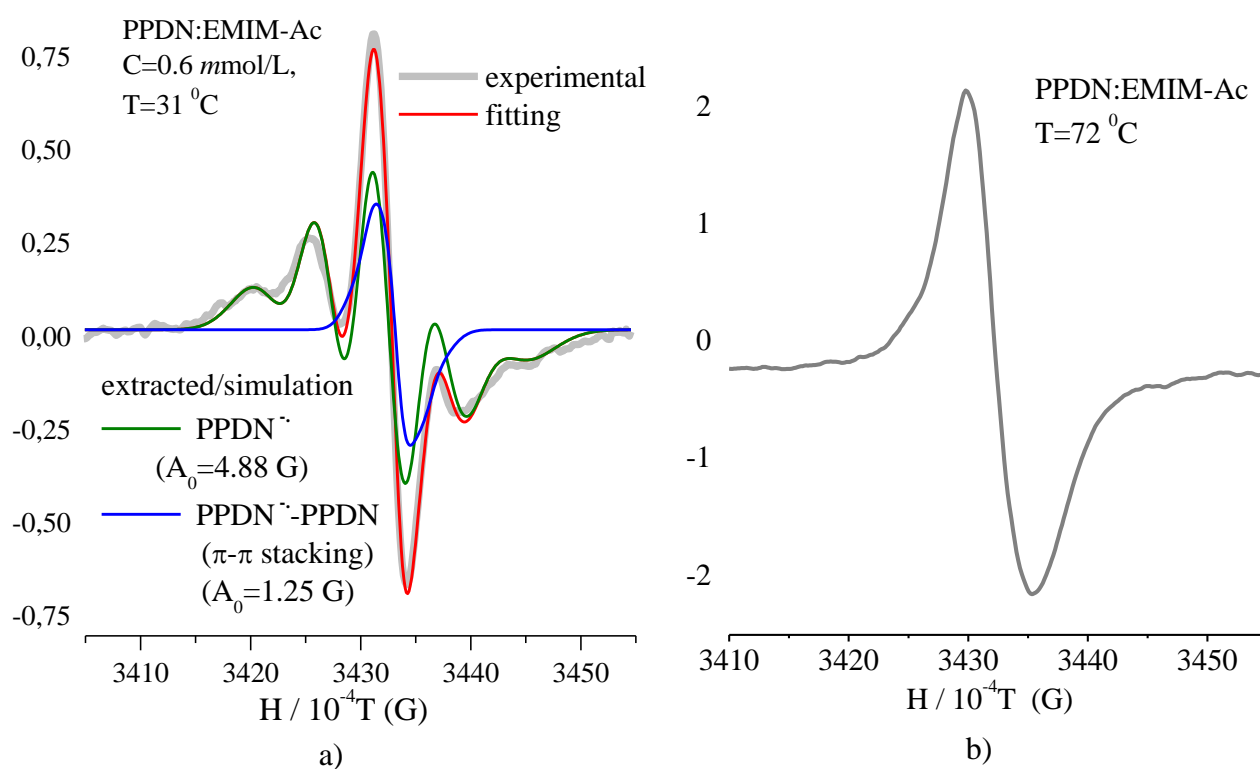


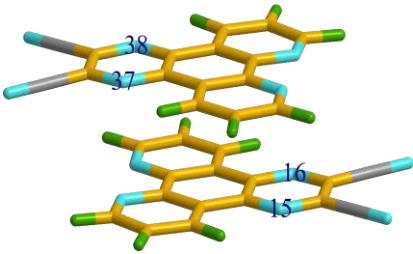
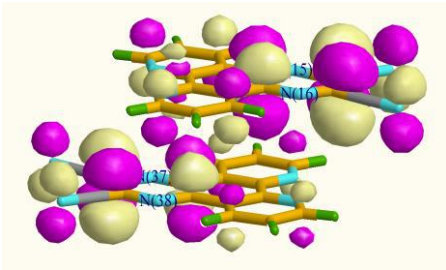
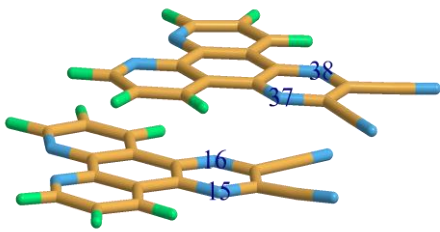
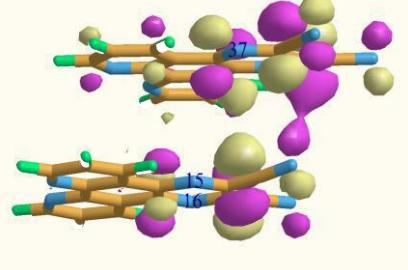
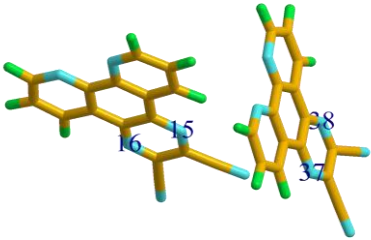
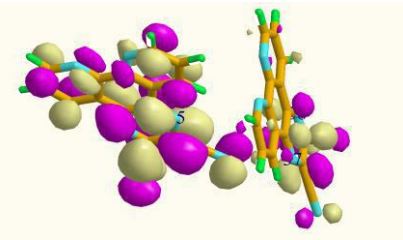
Fig.S5

PPDN:EMIM-Ac light induced EPR spectra recorded at: a) T=31 °C, the experimental as well as the fitted spectra are shown, b) recorded at T=72 °C, the spectrum demonstrates the complete degradation of PPDN \cdot and a manifold increase in the number of other radical products (see the intensity scale of the spectra recorded utilizing the same amount of the same sample and the same set of experimental conditions).

Some variants of different relative positions of two PPDN skeletons at the time of the collision as well as the appropriate calculated isotropic parameters (A_0) of two nitrogen pairs denoted by N(15, 16), N(37, 38) are introduced in table SM-1. Therefore, $F_{(D)}$ corresponds to the hfc spectrum that consists of two pairs of ^{14}N with close $A_{0(D)}$ ($I=4$, $2I+1=9$ hfc lines with an equilibrium degeneracy of 1:4:10:16:19:16:10:4:1). An essentially simplified approach for spectral processing of four equivalent ^{14}N nuclei, utilizing only 5 hfc lines (10:16:19:16:10) is justified, taking in mind the strong difference in integral intensity in accordance with the above

mentioned degeneracy and dependence of broadening versus $\sim m_i^2$ ($m_i=0,1,2,3,4$). An additional confirmation of the “free” electron hopping relates to the evaluation of the LUMO level, where molecular LUMO orbitals are overlapping in case of a π - π stacking structure (I-, II- models in Table S1). The mean values of DFT calculated $A_{0(D)} \approx 2$ G, $A_{0(M)} \approx 5$ G and respectively the experimental processing of $A_{0(D)} \approx 2.5$ G and $A_{0(M)} \approx 5.3$ G indicate that the frequency $\omega=1/\tau_1$ (τ_1 is the mean lifetime of a π - π stacked pair of $\text{PPDN}^{\cdot\leftrightarrow}\text{PPDN}$) of electron hopping should be faster than 10 MHz. The last data are surely supported, for instance, by X-band ENDOR measurements in covalent and self- assembled π - π stacked perylene diimides [S9].

Table SM-1. Some versions of dimer structures around π - π stacking ($\text{PPDN}^{\cdot\leftrightarrow}\text{PPDN}^{\cdot}$) morphology and isotropic A_0 constant evaluation in Gaussian (G-16) [S11].

PPDN Dimers		(A_0 /G)
		G-16/DFT/ B3YP/EPR-II ^{*)}
I-model, π - π stacking, MM2, force field E/S- opt. ^{**)} , LUMO- 3.561 eV		
		N(15) 1.99 N(16) 2.01 N(37) 2.00 N(38) 2.00
II-model π - π stacking, MM2, force field E/S-opt., LUMO -3.815 eV)		
		N(15) 2.11 N(16) 2.32 N(37) 1.43 N(38) 1.44
III-model S/E-opt. ^{**)} (G-16/DFT/B3YP/EPR-II (LUMO -3.577eV))		
		N(15) 2.15 N(16) 2.31 N(37) 2.00 N(38) 2.00

^{*)} -Basis set EPR-II, indicates a good correlation of the isotropic hfc constant value (A_0) with the experimentally derived for PPDN^{\cdot} . ^{**)} - E/S -opt. (energy/structure optimization)

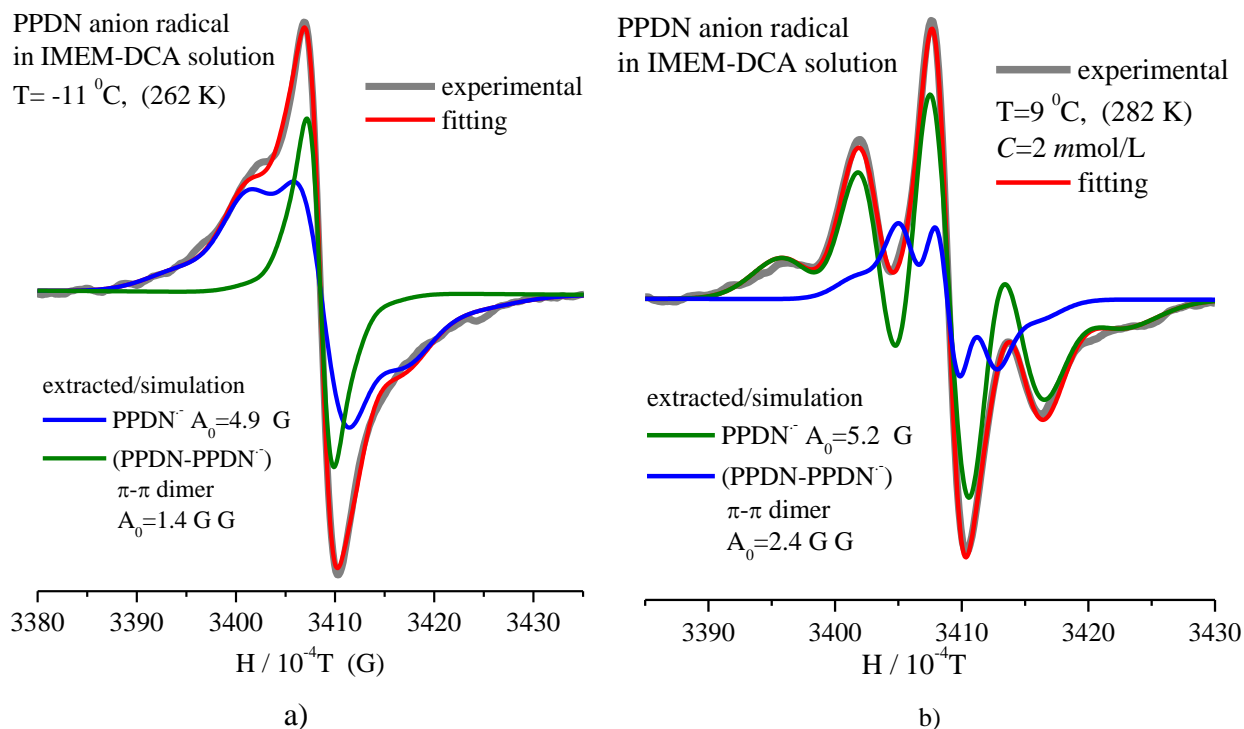


Fig. S5

Light induced EPR spectra of PPDN:EMIM-DCA solution ($C=2$ mmol/L) have been recorded at: a) $T=-11$ °C, b) $T=72$ °C. The processing based at the supposition of summarized contributions of the monomer and dimer spectra.

SM-2c. PPDN light-induced reaction kinetics

Below the following designations are utilized

N = PPDN,

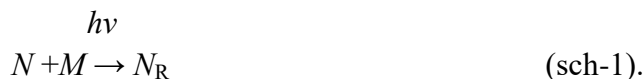
M = IL anion

N_R = PPDN \cdot^- (PPDN anion radical)

L – unknown reagent

P – unknown not paramagnetic product

The light-induced electron transfer from IL anions leads to PPDN molecule degradation via a second order reaction of PPDN and IL anions. Omitting here the consideration of M' radical generation one can write



Taking into account that $M \gg N$ and designating $k_{12} \cdot M = K_1$, the kinetics equation for N can be written as

$$\frac{dN}{dt} = -k_{12} \cdot (M - N) \cdot (N) \approx -k_{12} \cdot M \cdot N = -K_1 \cdot N \quad (\text{S1}),$$

and therefore (S1) has a simple solution

$$N = N_0 \cdot e^{-K_1 \cdot t} \quad (\text{S2})$$

Experiments, namely the sequential recording of spectra introduced in Fig.S5 indicate a relatively slow process at room temperature. The kinetics of the annihilation of the radical species are leading to a non-paramagnetic product formation. Assuming, that the process in (sch-1) is

irreversible, due to a high reactivity and therefore a fast recombination of M^* , we suppose the second order reaction N_R with an unknown reagent L is resulting in the formation of a non-paramagnetic product P



Once again assuming $[L] \gg [N_R]$ and designating $k_2 \cdot [L] = K_2$, the linear differential equation (*lde*) relatively N_R can be written as

$$\frac{dN_R}{dt} = K_1 \cdot N - k_2 \cdot N_R \cdot (L - N_R) \approx K_1 \cdot N - K_2 \cdot N_R \quad (\text{S3}),$$

or utilizing the general form for *lde*

$$\frac{dY}{dx} + P \cdot y = Q \quad (\text{S4})$$

(S3) can be overwritten as

$$\frac{d[N_R]}{dt} + K_2[N_R] = K_1[N] \quad \rightarrow \quad \frac{d[N_R]}{dt} + K_2[N_R] = K_1[N_0] \cdot e^{-K_1 t} \quad (\text{S5})$$

Where in (S4) $Y = N_R$, $x = t$, $P = K_2$, $Q = [N_0] \cdot K_1 \cdot e^{-K_1 t}$ (S5a)

Since the general solution of (S4) is $Y = e^{-\int P \cdot dx} \left[\int e^{\int P \cdot dx} \cdot Q \cdot dx + C \right]$ and using (S5a) with

the boundary conditions $Y=0|_{t=0}$, the solution of (S5) is written as follows

$$Y = e^{-K_2 t} \left[\int e^{K_2 t} \cdot N_0 \cdot K_1 e^{-K_1 t} dt + C \right] = e^{-K_2 t} \cdot \left[N_0 \cdot K_1 e^{(K_2 - K_1)t} dt + C \right]$$

$$Y = e^{-K_2 t} \cdot \left[\int N_0 \cdot K_1 e^{(K_2 - K_1)t} dt + C \right] = e^{-K_2 t} \cdot \left[\frac{N_0 \cdot K_1}{(K_2 - K_1)} e^{(K_2 - K_1)t} + C \right]$$

$$Y = 0|_{t=0}, \quad \frac{N_0 \cdot K_1}{K_2 - K_1} + C = 0, \quad C = -\frac{N_0 \cdot K_1}{K_2 - K_1}$$

$$Y = e^{-K_2 t} \cdot \left[\frac{N_0 \cdot K_1}{K_2 - K_1} e^{(K_2 - K_1)t} - \frac{N_0 \cdot K_1}{K_2 - K_1} \right] = N_0 \cdot \frac{K_1}{K_2 - K_1} (e^{-K_1 t} - e^{-K_2 t})$$

Therefore, the experimentally derived kinetics of N_R should be described by the known expression for a simple consequent generation/annihilation in molecular reactions

$$N_R = N_0 \cdot \frac{K_1}{K_2 - K_1} (e^{-K_1 t} - e^{-K_2 t}) \quad (\text{S6})$$

Taking into account, that the summarized concentrations of all considered products of the current reactions here are equal to the initial concentration of PPDN, i.e. $N_0 = N + N_R + P$ and using (S2) and (S6) one can get

$$P = N_0 \left[1 - \frac{K_2 \cdot e^{-K_1 t} - K_1 \cdot e^{-K_2 t}}{K_2 - K_1} \right] \quad (\text{S7})$$

The formation of P under the light excitation, is connected with the irreversible change of the molecular structure of PPDN or the formation of composites that include the base molecule. This is indirectly confirmed by the optical absorption measurements on PPDN:BMIM-BF₄ and EMIM-DCA solutions at room temperature before and after Xe-lamp excitation. However, the above mentioned assumptions should be clarified via chemical analysis, as a minimum, and by means of NMR. The PPDN absorption spectrum in organic solvents includes well resolved, characteristic intensive lines at wavelengths around 307 nm, [S10] and two weaker at around 347 nm and 365 nm in BMIM:BF₄. The lines at respectively 319 nm, 351 nm and 367 nm were detected in EMIM-

DCA solution. After illuminating a 0.02 mm layer of solution placed between two quartz (Q-z) plates for 5 minutes with a continuous Xe lamp, these lines lost about 90% of their initial intensity in BMIM-BF₄, as shown in Fig.S6a and about 50% in EMIM-DCA solution after 4 minutes of Xe-lamp illumination (Fig.S6b). In order to be sure that Xe-lamp light power density ($< 30 \text{ mW/cm}^2$) does not initiate the degradation of the utilizing here ILs the same experiments were carried out at the same conditions but only with ILs and the example of BMIM-BF₄ data are shown in Fig.6a (S₁, S₂). One can see an absence of IL spectra changing in range $300 \text{ nm} < \lambda < 400 \text{ nm}$ after Xe-lamp illumination. Note, that UV-spectra calculation in ORCA, utilizing hybrid functional B3LYP and the def2 basis sets (Def2-TZVP, f-polarization functions) gives the good correlation of experimental and calculated data, that is confirmed by the lines position in range $300 \text{ nm} < \lambda < 400 \text{ nm}$ namely 301, 309 nm and 363 nm in Fig.6a. Note that in EMIM-DCA the spectra (Fig.6b) indicate some difference in resonance line positions as mentioned above, but any additional lines attributed to the EMIM-DCA degradation has not been detected as well. Thus, the EPR confirms the result in the PPDN samples due to the absence of spectra in the illuminated PPDN solution after a time close to that calculated by equation (S6). The results of processing the reaction kinetics are shown in Fig. 7a,b,c,d. Note, that the NR \sim EPR amplitude $A(t)$, i.e. in the case of PPDN for the HF line $m=0$, the double integral of the experimental EPR spectra is proportional to $A(t)$, of course, assuming that $\Delta H_m=0$ weakly depends on temperature, due to $\alpha_{\text{hfc}} \gg \alpha_1$, as was indicated in the main text of the manuscript.

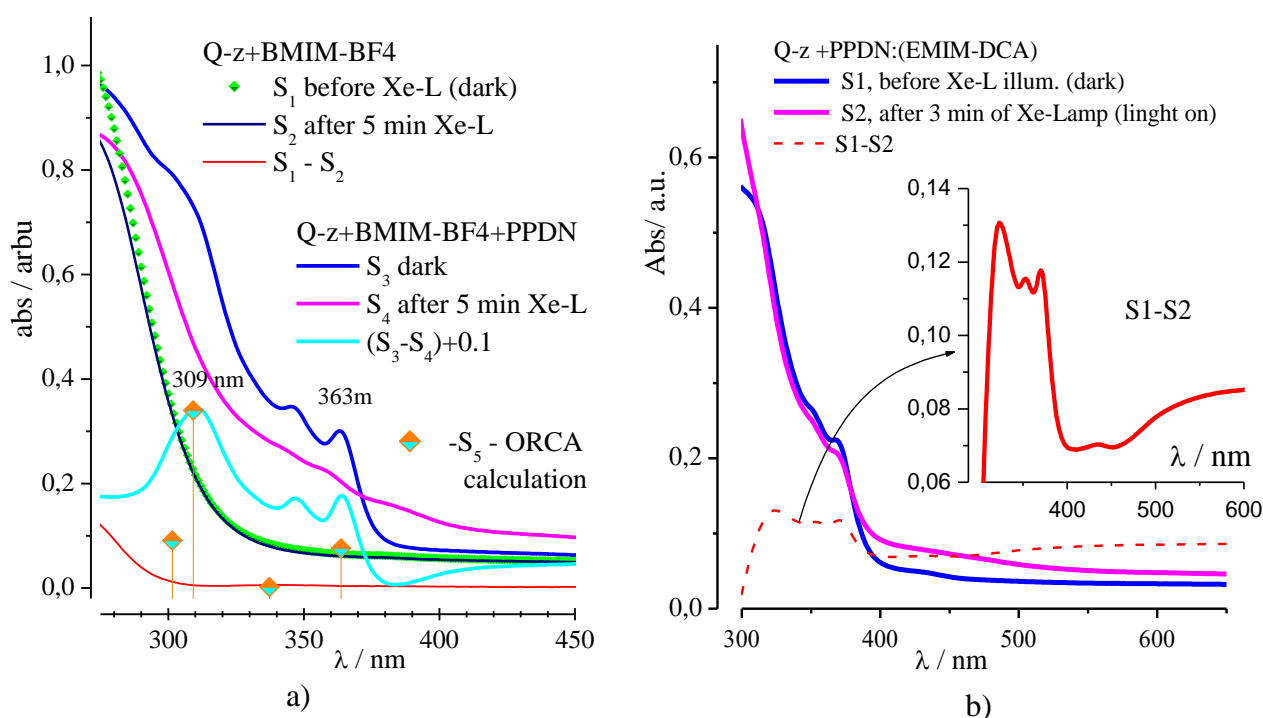


Fig.S6

PPDN absorption spectra in a) BMIM-BF₄ and b) EMIM-DCA solutions. Other appropriate information is placed in the text and in the inserts in the figures.

Regarding to the kinetical model, the expressions (S2, S6, S7) reliably describe the experimental results, that predict the system states (N , N_R , P) quantitatively at any point in time during the reaction. The evaluation of the temperature dependence of the molecular reaction rate constants K_1 , K_2 via consideration of three basically possible variants, can be expressed in a general form as:

$$K(T) = CT^\theta e^{-\frac{\Delta E}{T}} \quad (\text{S8})$$

where C is a constant, ΔE [in K] describes the energetic barrier that has to be overcome for an initiation of the reaction, and θ has slightly different meanings varying with the according theories, in this case in particular $\theta = 0, 0.5, 1$ - corresponding respectively to the Arrhenius, collision, and transition state theories.

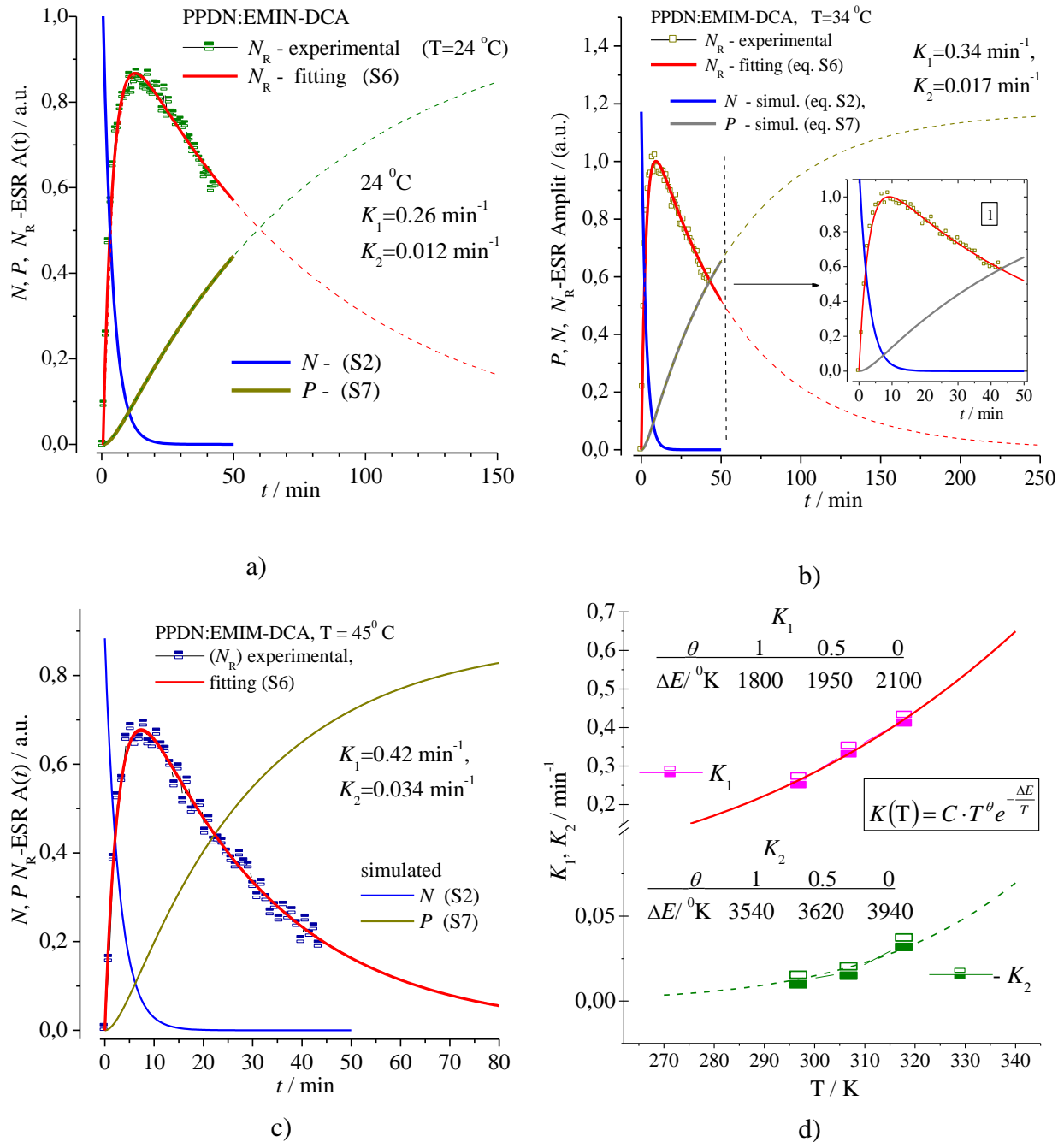


Fig.S7

a), b), c) - $A(t)$ – light-induced ESR amplitude of PPDN $^+$ spectrum (hfc line $m=0$), versus time t , recorded at 24°C , 34°C , and 45°C , d) the rate constants K_1, K_2 dependencies versus temperature. The appropriate spectra processing has been carried out by expressions (S2), (S6), (S7) and (S8).

SM-2d. Some comments concerning PPDN solutions

Impurities in the respective RTILs with concentrations $<5\%$ cannot be reliably detected here from the EPR spectra of PPDN. The corresponding data are given, for example, in Fig. 8 of the main text, where in a mixed solution of EMIM-DCA/ethanol, ethanol is a suitable model component of a liquid "impurity", given that the viscosities of the mixed solutions differ by about an order of magnitude, at least in the temperature range used in the experiments (~ 14.6 mPas and ~ 1.53 mPas, respectively, at 295 K). Indeed, according to the data shown in Fig. 8, the "impurity" of 5% ethanol ($X_2=0.05$) changes η by approximately 1 mPas or $\sim 6.6\%$ of the hypothetical impurity-free EMIM-DCA, which corresponds to a change in δ_1 by ~ 0.02 mT (~ 0.002 G), as follows from the dependence $\delta_1 = F(T)$ along the left axis in Fig. 8, i.e. from 0.03 mT to 0.028 mT. This value is comparable to $\Delta\delta_1 \approx 6-8\%$, due to the processing accuracy $\delta_1 = F(T)$ obtained by fitting. The latter is a reason that can limit the accuracy of the estimation of impurities that affect the reaction kinetics, which directly depends on η . It should be emphasized that the above estimate refers to 5% impurities, and working solutions correspond to a maximum of 2%. These concentrations could be available only in rare cases associated with a strong influence of impurities on the physical properties of the IL. Based on the above numerical evaluation, it is assumed that data similar to those presented in Fig. 8 of the main text can be used to determine the upper limit of impurity concentrations, namely those that can affect the effective spin relaxation time of the RA investigated in this work.

SM-2e. PPDN^{-•} spectra in EMIM-DCA solution introduced in Fig 2.

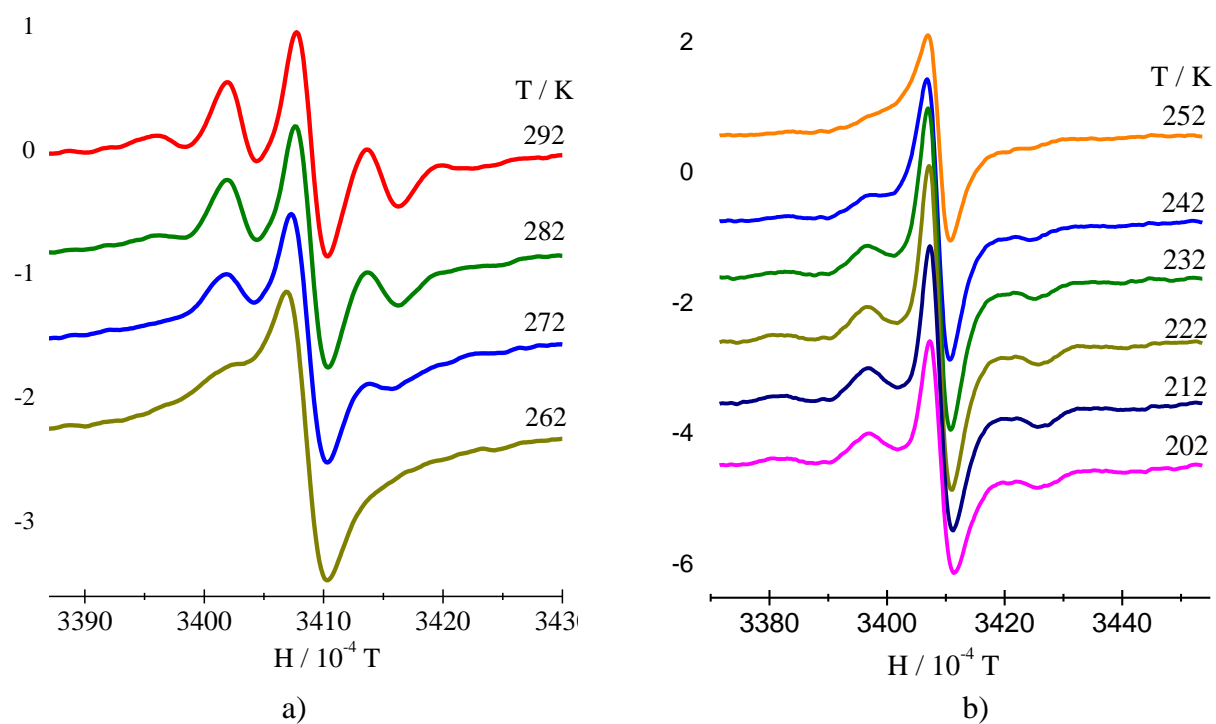


Fig. S8

PPDN^{-•} spectra in EMIM-DCA solution recorded below and higher of the freezing temperature $T_f = 252$ K: a) $T_i > 252$ K, and b) below $T_j < 252$ K

SM-3. NTCDA.

SM-3a. Some details concerning the NTCDA solutions

The concentrations allowing for the independent determination of τ_c and k_{ex} separately, has been determined and occupy the range $0.5 < C < 6$ mmol. The contribution from the *EA* solid phase in blends with $C < 6$ mmol to the effective relaxation assigned to the kinetics of photoreaction in utilizing $\text{NTCDA}^{\bullet-}$ solutions has not been found. The latter is confirmed by the comparison of two central ($m=0$) lines of $\text{NTCDA}^{\bullet-}$ EPR spectra in BMIM-BF₄ solutions, introduced in Fig.S9.

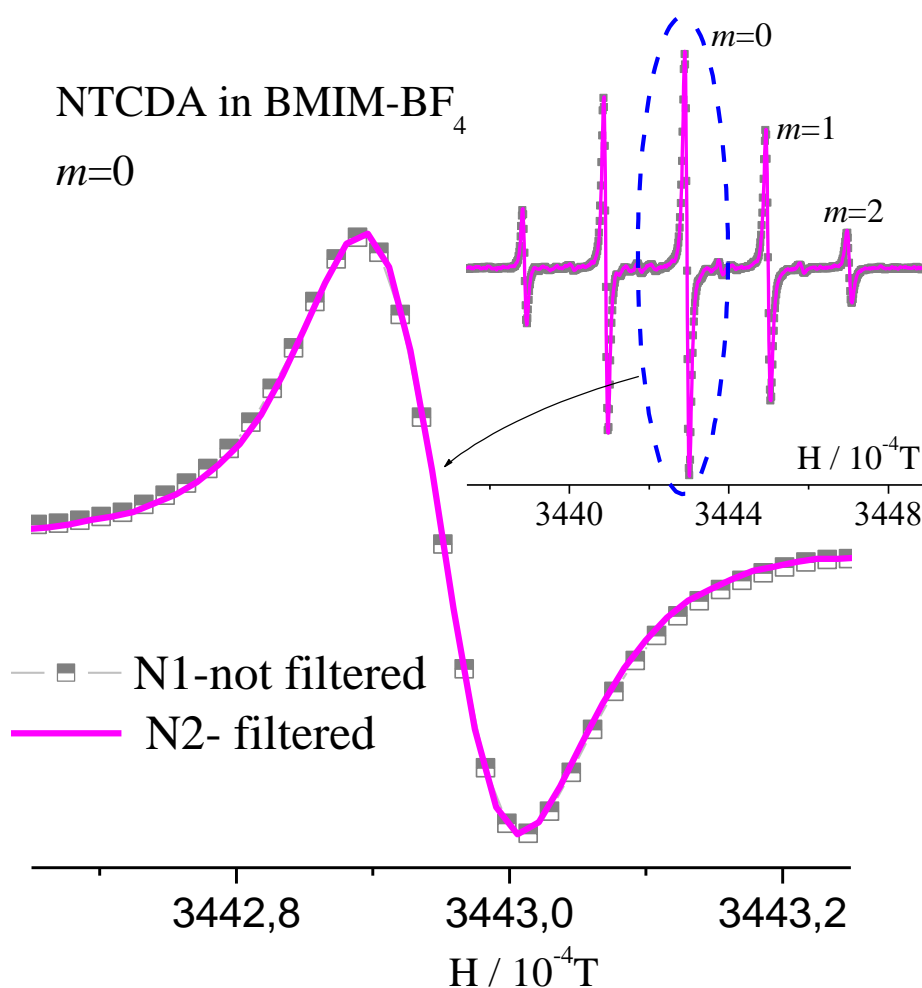


Fig. S9

N1 refers to the solution with the basic concentration $C=5$ mmol and N2- is the filtered N1 with the pore size of filter $0.2 \mu\text{m}$. The same result has been detected in $\text{PPDN}^{\bullet-}$ solutions.

SM-3b. Some sets of $\Delta H_{(m)}$ least-squares analysis

The dipolar contribution α_{dd} in $\alpha_o = \alpha_{ex} + \alpha_{dd} + \alpha_{in}$ is responsible for the hfc line broadening and it has the same activation mechanism as α_1 related to the rotational motion of radicals (the same exponential sign). Therefore, in case of the close values of their activation energies, there is some uncertainty in the correct E_η and E_t determination. However, taking in mind that in (11) $A_1 \cdot B_1 = P_1 \cdot P_2 = q$, which is a constant for radicals with the same C , f_m , S , one can use q value for an analogical radical, which was taken from literature. For instance, using the TEMPOL data (reference [37] in the main text) with the appropriate correction of C and f_m ($G=6$ instead of $G=1$) one can get $q \approx 550 \text{ G}^2/(\text{mol/L})^2$. Utilizing the working expression for the $(\alpha_o + \alpha_1)$ temperature dependence,

$$\alpha_1 + \alpha_o = a \cdot \frac{e^{E_\eta/T}}{T} + C \cdot \left[\frac{q}{A_1} e^{(E_r/T)} + A_1 \cdot e^{(-E_r/T)} \right] + \alpha_{in} \quad (\text{S9})$$

the fitting procedure for the solution with $C = 1.9 \cdot 10^{-3} \text{ mol/L}$ (Fig.13), gives $A_1 = 1.96 \cdot 10^6 \text{ G}/(\text{mol/L})$, $E_\eta' = 2600 \text{ K}$, $E_t' = 3150 \text{ K}$, $a \approx 7.8 \cdot 10^{-4} \text{ G} \cdot \text{T}$, $\alpha_{in} = 0.03 \text{ G}$. The same fitting for $C = 9.5 \cdot 10^{-4} \text{ mol/L}$ (Fig.S10), with the above a and A_1 , as fixed parameters gives $E_\eta' = 2270 \text{ K}$, $E_t' = 3240 \text{ K}$ and $\alpha_{in} = 0.037 \text{ G}$ and indicates that the deviation between the activation energies obtained for both C does not exceed 3.5%. Note that $\alpha_{in} \approx 0.03 \text{ G}$ was obtained via processing of (S9). This coincidences with the one obtained from the linear $Y(C)$, shown in insert 1 in Fig.S10, i.e. $\alpha_{in} \approx 0.029 \text{ G}$ (the caption of Fig.S10).

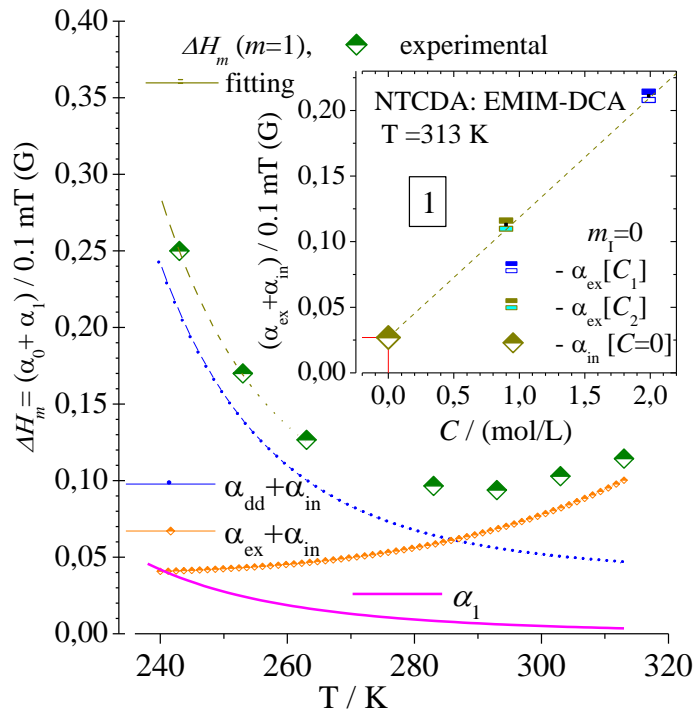


Fig.S10

Experimental and fitted graphs for $\Delta H_{(m=1)} = \alpha_{ex} + \alpha_{dd} + \alpha_{in} = F(T)$ of the hfc EPR spectrum line ($m=1$, $G=4$), obtained in NTCDA \cdot^- :EMIM-DCA solution at 313 K. In insert 1, the experimental and fitted linear functions $Y(C) = \chi \cdot C + \alpha_{in}(C=0)$ with $\chi = 0.09 \text{ G}/(\text{mol/L})$ and $\alpha_{in} = 0.029 \text{ G}$ are shown.

SM-3c. The comparison of PPDN^{-•} and NTCDA^{-•} α , β , δ with the same for nitroxides

g- and A- of the typical nitroxide

$$g_x = 2.0024, g_y = 2.0067, g_z = 2.0097, A_x = 7.2 \text{ G}, A_y = 5.8 \text{ G}, A_z = 34.3 \text{ G}$$

$$\Delta g_N = g_z - (g_x + g_y)/2 = 5.15 \cdot 10^{-3}, \quad \Delta A_N = A_z - (A_x + A_y)/2 = 27.8 \text{ G}$$

while for PPDN^{-•}

$$\Delta g_{\text{PPDN}} = g_z - (g_x + g_y)/2 = 1.6 \cdot 10^{-3}$$

Therefore $\Delta g_N / \Delta g_{\text{PPDN}} = 3.22$ and

$$(\Delta g_N / \Delta g_{\text{PPDN}})^2 = 10.36$$

i.e. the contribution to α_1 depending from $(\Delta gH)^2$ in nitroxides exceeds more than an order of magnitude in both, PPDN^{-•} and NTCDA^{-•}.

As for the data for nitroxides and PPDN given in the table below, one can see approximately the same contributions to the width of the hfc lines, at least for the boundary lines related to the m^2 maximum:

$$\text{PPDN}^{-\bullet} \quad m=2, \quad m^2 \cdot \delta = 4 \cdot 33 = 132$$

$$\text{Nitroxides} \quad m=1, \quad m^2 \cdot \delta = 1 \cdot 96 = 96$$

Table

X-Band ($m_I = 0$)		α/γ	β/γ	δ/γ
PPDN^{-•}				
$A_X = -0.33$ $A_Y = -0.36$ $A_Z = 15.8$	$g_x = 2.0039$ $g_y = 2.0037$ $g_z = 2.0022$	55	21.7	33
NTCDA^{-•}				
$A_X = -2.33$ $A_Y = -0.33$ $A_Z = -2.7$	$g_x = 2.00224$ $g_y = 2.00416$ $g_z = 2.00417$	4.7	1.2	0.9
(Typical Nitroxide)[•]				
$A_X = -7.2$ $A_Y = 5.8$ $A_Z = 34.3$	$g_x = 2.0024$ $g_y = 2.0067$ $g_z = 2.0097$	143	140	96

NTCDA^{-•} is suitable for the spin-spin or chemical exchange study due to the slight anisotropy of the hfc parameters.

SM-3d. NTCDA data $D_t = F(T)$ in EMIM-DCA and BMIM-BF₄ solutions presented in Fig. S11 were estimated by (14) using the results of α_{ex} shown in Fig. 13 and Fig. 14.

Note : (14), Fig.13, Fig.14 are referred to the main text

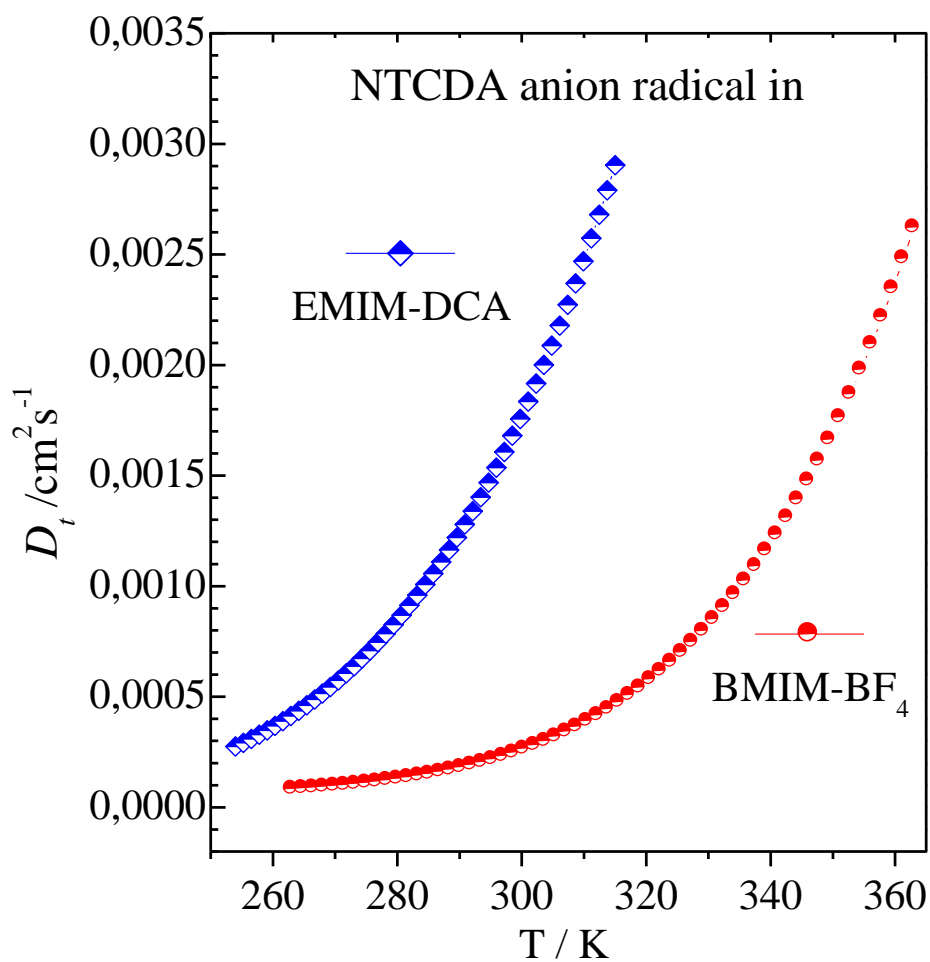


Fig S11

$D_t = F(T)$ of : a) NTCDA^{-•}:EMIM-DCA ($C=3 \cdot 10^{-3}$ mol/L) and
b) NTCDA:BMIM-BF₄ ($C=7 \cdot 10^{-4}$ mol/L) solutions.



O/P 29

Interaction between 1-butyl-3-methylimidazolium acetate ionic liquid and polymer positive polaron: ESR detection under Xe-lamp excitation at 77K

A.L. Konkin¹, U. Ritter¹, P. Scharff¹, A. Aganov², A.A. Konkin², V. Krinichnyi³

¹ Center for Micro- and Nanotechnologies, Ilmenau University of Technology, D-98693 Ilmenau, Germany

² Institute of Physics, Kazan Federal University, Krem. 18, Kazan, Russia

³ Department of Kinetics and Catalysis, Institute of Problems of Chemical Physics, Semenov Avenue 1, Chernogolovka, Russia

* corresponding author: e-mail: alexander.konkin@tu-ilmenau.de

Keywords: ESR, ionic liquid, organic solar cells

Abstract

The formation of methyl radicals in a suspension of the donor/acceptor pair PCDTBT:PC₆₀BM (Fig.1 a,b) in di-chloro-benzene (dCB) and 1-butyl-3-methylimidazolium acetate (Fig.1c) as ionic liquid (IL) has been recorded at 77K temperature under UV illumination of a continuous waves Xe-lamp (30 mW/cm²; output power density). The ESR X-band spectrum of the above blend is shown in Fig.2.

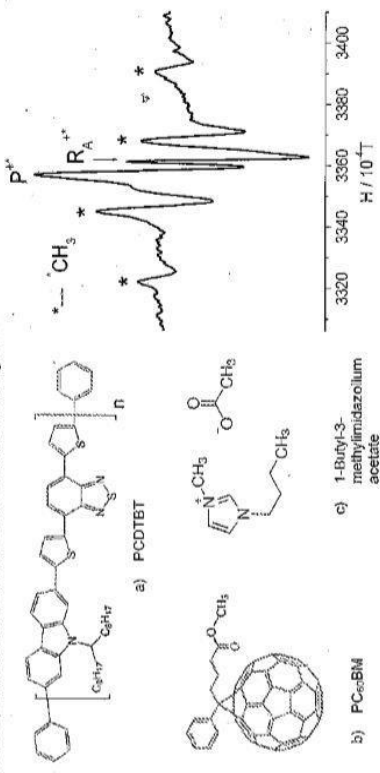


Fig.1.

Structures of: a) electron donor (PCDTBT), b) acceptor (PC₆₀BM) and c) imidazolium based IL.

Fig.2.

ESR spectrum of PC₆₀BM:PCDTBT (1:1) solution in dCB + IL, recorded after 20 minutes of (~30 mW/cm²) Xe-lamp illumination at 77K. P⁺, and R_A⁺ are the positive polaron and fullerene anion radical respectively.

Taking into account that methyl radicals were not found in pure 1-butyl-3-methylimidazolium acetate under the same conditions of illumination, it was supposed that acetate anion interacts with the positive PCDTBT polaron due to the electron transfers to the polymer and therefore polaron annihilation.



References

- [S1]. C.A. Reed, R.D Bolskar, Discrete Fulleride Anions and Fullerenium Cations, *Chem. Rev.* 100 (2000) 1075-120
- [S2]. A. StaSko, V. Brezovfi, S. Biskupie, K.-P. Dinse, P. Schweitze, M. Baumgarten, EPR Study of Fullerene Radicals Generated in Photosensitized TiO₂ Suspensions, *J. Phys. Chem.* 99 (1995) 8782-8789
- [S3]. J. A. Mikroyannidis , A. N. Kabanakis , S. S. Sharma , G. D. Sharma, Dumb-belled PCBM derivative with better photovoltaic performance, Dumb-belled PCBM derivative with better photovoltaic performance, *Adv. Funct. Mater.* 21 (2011) 746–755
- [S4]. J. Niklas, K. L. Mardis, B. P. Banks, G. M. Grooms, A. Sperlich, V. Dyakonov, S. Beaupre, M. Leclerc, T. Xu, L. Yu, O.G. Poluektov, Highly-efficient charge separation and polaron delocalization in polymer–fullerene bulk-heterojunctions: A comparative multi-frequency EPR and DFT study, *Phys. Chem. Chem. Phys.*, 15 (2013) 9562- 9574
- [S5]. B. Kosan, C. Michels, F. Meister, Dissolution and forming of cellulose with ionic liquids *Cellulose*, 15 (2008) 59–66
- [S6]. Q. L. Kuang, J. C. Zhao, Y. H. Niu, J. Zhang, Z. G. Wang, Celluloses in an ionic liquid: the rheological properties of the solutions spanning the dilute and semidilute regimes *J. Phys. Chem. B* 112 (2008) 10234–10240.
- [S7]. R. J Sammons, J. R. Collier, T. G. Rials, S. Petrovan, Rheology of 1-butyl-3-methylimidazolium chloride cellulose solutions. I. Shear rheology *J. Appl. Polym. Sci.* 110 (2008), 1175-1181
- [S8]. a) A. K. Vijn , B. E. Conway, Electrode Kinetic Aspects of the Kolbe Reaction, *Chem. Rev.* 67 (1967) 623–664
 b) B. Smaller, M. S. Matheson, Paramagnetic Species Produced by γ Irradiation of Organic Compounds, *J. Chem. Phys.* 28 (1958) 1169-1178
- [S9]. M. R. Wasielewski, Self-Assembly Strategies for Integrating Light Harvesting and Charge Separation in Artificial Photosynthetic Systems, *Acc. Chem. Res.* 42 (2009) 1910-1921
- [S10]. N. Thejo Kalyani, S.J. Dhoble, Novel materials for fabrication and encapsulation of OLEDs, *Renew. Sust. Energ. Rev.* 44 (2015) 319–347
- [S11]. Gaussian 16, Revision B.01, M. J. Frisch, G. W. Trucks, H. B. Schlegel, G. E. Scuseria, M. A. Robb, J. R. Cheeseman, G. Scalmani, V. Barone, G. A. Petersson, H. Nakatsuji, X. Li, M. Caricato, A. V. Marenich, J. Bloino, B. G. Janesko, R. Gomperts, B. Mennucci, H. P. Hratchian, J. V. Ortiz, A. F. Izmaylov, J. L. Sonnenberg, D. Williams-Young, F. Ding, F. Lipparini, F. Egidi, J. Goings, B. Peng, A. Petrone, T. Henderson, D. Ranasinghe, V. G. Zakrzewski, J. Gao, N. Rega, G. Zheng, W. Liang, M. Hada, M. Ehara, K. Toyota, R. Fukuda, J. Hasegawa, M. Ishida, T. Nakajima, Y. Honda, O. Kitao, H. Nakai, T. Vreven, K. Throssell, J. A. Montgomery, Jr., J. E. Peralta, F. Ogliaro, M. J. Bearpark, J. J. Heyd, E. N. Brothers, K. N. Kudin, V. N. Staroverov, T. A. Keith, R. Kobayashi, J. Normand, K. Raghavachari, A. P. Rendell, J. C. Burant, S. S. Iyengar, J. Tomasi, M. Cossi, J. M. Millam, M. Klene, C. Adamo, R. Cammi, J. W. Ochterski, R. L. Martin, K. Morokuma, O. Farkas, J. B. Foresman, and D. J. Fox, Gaussian, Inc., Wallingford CT, 2016.